Original Research

TiO$_2$ nanosheets synthesized by atomic layer deposition for photocatalysis

Riyanto Edy[a,b], Yuting Zhao[b], Gaoshan S. Huang[b], Jianjun J. Shi[c,*], Jing Zhang[c], Alexander A. Solovev[b], Yongfeng Mei[b]

[a] State Key Laboratory for Modification of Chemical Fibers and Polymer Materials, College of Material Science and Engineering, Donghua University, Shanghai 201620, China
[b] Department of Materials Science, Fudan University, Shanghai 200433, China
[c] College of Science, Donghua University, Shanghai 201620, China

ABSTRACT

Two-dimensional TiO$_2$ nanosheets were synthesized by atomic layer deposition (ALD) on dissolvable sacrificial polymer layer. The photocatalytic performance of free-standing TiO$_2$ nanosheets prepared with different numbers of ALD cycles (100, 300, 500, and 1000) were investigated by evaluating the degradation rates of methyl orange solutions. It is shown that the photocatalytic activity increases due to Ti^{3+} defect and the locally ordered structures in amorphous TiO$_2$ nanosheets. The difference in the surface areas of nanosheets may also play a crucial role in the photocatalytic activity. The results obtained in this work can have potential applications in fields like water splitting and dye-sensitized solar cells.

1. Introduction

Atomic layer deposition (ALD) has become advanced fabrication method for a rich variety of applications including complementary metal oxide semiconductor transistors, DRAM memory, energy conversion, photovoltaic, and display devices [1–6], which require a precise control of thickness, uniformity, and conformality. Recently, novel application of ALD includes synthesis of two-dimensional (2D) nanosheets [7]. 2D nanosheets have emerged as important new materials due to their unique structural, morphological, and physico-chemical properties with attractive functionalities [8–15]. On the other hand, since Fujishima and Honda found that TiO$_2$ can split water to generate hydrogen in 1972 [16], TiO$_2$ has been widely used in energy and environmental science due to its high chemical stability, non-toxicity and favorable energy band structure [17–20]. As we know, the properties of nanomaterials depend on their shapes, sizes, crystal phases, defects, impurities, and surface areas, and their potential applications will also be strongly influenced [21–23]. In this study, 2D catalytic TiO$_2$ nanosheets fabricated by ALD on dissolvable sacrificial polymer layer were investigated. Photocatalytic properties of TiO$_2$ nanosheets were studied by evaluating the degradation rates of methyl orange (MO) solutions. The results indicate that photocatalytic performance increases with the thickness of nanosheet, and superficial Ti^{3+} defect while locally ordered structure in the amorphous TiO$_2$ plays an important role.

2. Experimental

In this work, TiO$_2$ was deposited by ALD on sacrificial polymer layer. The polymer layer of polyvinyl alcohol (PVA) with average molecular weight of ~ 89,000–98,000 was prepared by spin coating on 2×2 cm^2 silicon wafers at a rotational speed of 3000 rpm for 30 s (Fig. 1a). The PVA layer was baked on the hot plate at 100 °C for 60 s. During ALD, the precursor used for the Ti source was Tetrakis (dimethylamido) titanium (TDMAT) with added water (H$_2$O) as reactant. Both TDMAT and H$_2$O were exposed in the ALD chamber with the pulse and the purge times of 20 ms and 20 s, respectively. The ALD chamber temperature was set to 150 °C and the temperatures of TDMAT and H$_2$O were 105 and 50 °C, respectively. The flow rate of the carrier gas (N$_2$) was 20 sccm and the deposition was conducted at ~20 Pa. In this work, ALD of 100, 300, 500, and 1000 cycles were prepared to investigate the influence of layer's thickness. To obtain free-floating 2D TiO$_2$ sheets, the samples were scratched into small pieces and then immersed into the hot water of 75 °C (Fig. 1b-c). After 4 h, the PVA sacrificial layer was dissolved, while the free-standing TiO$_2$ nanosheets were released (Fig. 1d).

Morphologies of the TiO$_2$ nanosheets were investigated using optical microscopy (Olympus BX51) and scanning electron microscopy (SEM, Phenom world). Atomic force microscopy (AFM; Nanoscope IV SPM, Veeco Metrology) was used to examine the surface morphology and measure thicknesses of nanosheets. The crystal structures of the
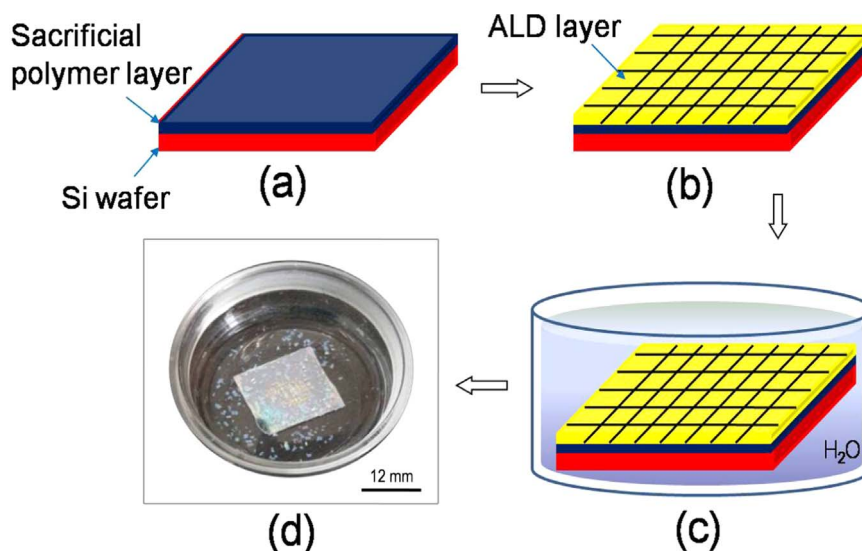
Fig. 1. Schematic diagram illustrating fabrication process of ALD nanosheets. (a) Spin-coated sacrificial polymer layer on silicon wafer. (b) TiO$_2$ layer was prepared on sacrificial layer by ALD and then scratched into small pieces by razor edge. (c) Sample was immersed in hot water to dissolve the sacrificial layer. (d) Typical optical image of the nanosheets after release (in Petri dish).

TiO$_2$ nanosheets were evaluated by X-ray diffraction (XRD) spectroscopy on a D8 spectrometer (Advance Bruker AXS GMBH), using CuKα radiation with irradiations condition of 40 kV and 40 mA. XPS experiments were carried out on a RBD upgraded PHI-5000C ESCA system (Perkin Elmer) with Mg Kα radiation (hν=1253.6 eV) and the X-ray anode was run at 250 W.

The photocatalytic performance of TiO$_2$ nanosheets was studied by photodegradation of MO solution measured by UV–Vis spectrophotometer (Shimadzu UV-2550). The TiO$_2$ nanosheets with the weight of 0.1 mg were placed in 6 mL MO solution (10 mg/L). The mixture was then kept in the dark for 30 min to achieve the adsorption equilibrium and then illuminated under the UV light of a 200-W xenon lamp (Lanpu, China) at a distance of 50 cm. The degradation of the MO solution was measured every 30 min. The absorption intensity at the wavelength of 464 nm (the maximum absorption peak of MO) [24] was extracted to calculate the MO degradation.

3. Results and discussion

Fig. 1 shows fabrication process of TiO$_2$ nanosheets. The release of nanosheets was achieved by dissolving PVA sacrificial layer in hot water. Scratching was used to accelerate the dissolution process of the PVA layer (Fig. 1a-c). To further speed up the release process, water was heated to 75 °C. The TiO$_2$ layer was separated from the sacrificial

layer and floated on the surface of water, as shown in Fig. 1d. The dissolution rate of the sacrificial polymer layer depends on chemical composition, molecular weight, and temperature of the solvent. Poly(acrylic acid) sacrificial layer with high solubility and low molecular weight led fast dissolution in water and corresponding high stress, causing the thin layer to break into very small pieces [7]. On the other hand, PVA showed good solubility in water with slower dissolution speed that allowed the above ALD layer to peel off gently. It enabled the formation of relatively large nanosheets with dimensions of several millimeters for subsequent collection and analysis.

Fig. 2 show the SEM images of TiO$_2$ nanosheets of (a) 100 and (b) 500 ALD cycles. In Fig. 2a, a thin TiO$_2$ nanosheet formed with 100 ALD cycles shows a typical flexible nanosheet. It can be transformed into a stiffed nanosheet by increasing the thickness as shown in Fig. 2b. Further evaluation can be seen in Supporting Information (Fig. SI-1), which shows free-floating/free-standing TiO$_2$ nanosheets in water. The TiO$_2$ nanosheets in Fig. SI-1a-1d were prepared by 100, 300, 500, and 1000 ALD cycles, respectively. Thinner TiO$_2$ nanosheets with fewer ALD cycles showed higher flexibility clearly indicated by wrinkling, rollable edges, and overlapping with self-folded layers (Figs. SI-1a and SI-1b). Thicker TiO$_2$ nanosheets with 500 and 1000 ALD cycles led to stiffer sheets. The robustness of the nanosheet makes it possible to keep the original rectangular shape, as shown in Figs. SI-1c and SI-1d.

We also experimentally proved that the increase of ALD cycles (i.e.
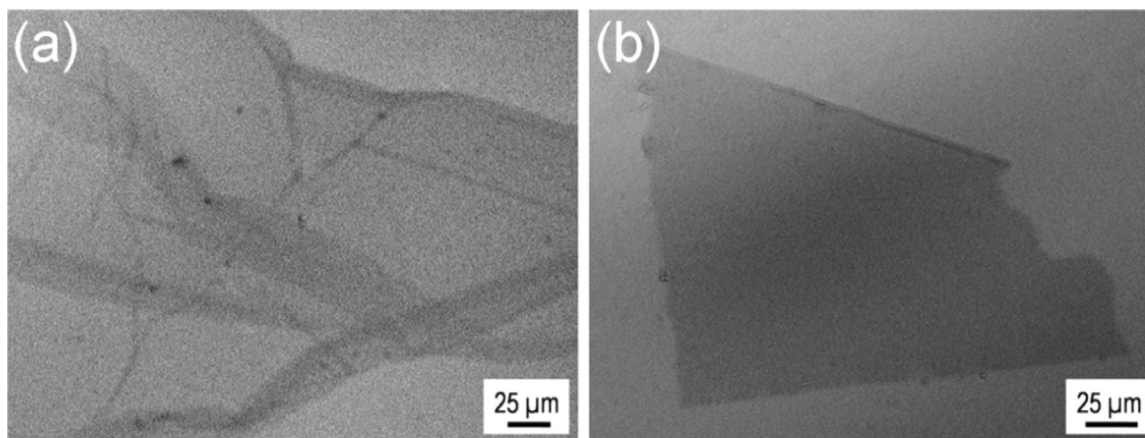

Fig. 2. SEM images of TiO$_2$ nanosheets fabricated by (a) 100 and (b) 500 ALD cycles.

thickness of the nanosheet) will enlarge dimensions of resulting nanosheets (Fig. SI-3, Supporting Information). The nanosheets in the water were dried and annealed (300 °C for 1 h) for further characterization. Fig. SI-2 in Supporting Information shows a typical morphology of the dried TiO_2 nanosheets. The contrast/different colors in various regions originates from optical interference due to the stacking or overlap of nanosheets since the TiO_2 nanosheets fabricated with fewer ALD cycles are more flexible. On the contrary, the nanosheets fabricated with more ALD cycles are stiffer (Fig. SI-2 and SI-3 in Supporting Information). We believe that the stiffer nanosheets may have more regular repetitive patterns of the atoms although the nanosheets are amorphous phase [25–27]. This local ordering in the amorphous TiO_2 is considered to be due to the highly directional covalent bonds [28,29].

In our experiment, we noticed that ALD of TiO_2 causes morphology evolution. Fig. SI-4 of Supporting Information shows surface morphologies of the uncoated PVA layer and the ALD TiO_2 nanosheets with various thicknesses on PVA sacrificial layer. It reveals that the TiO_2 layers are much smoother than bald PVA layers. It correlates to the typical ALD growth mechanism onto the PVA surface. When the TiO_2 ALD layer was deposited onto the PVA surface, TDMAT exposure consumes OH groups and produces $Ti-(N(CH_3)_2)_3$ [30,31]. The reactive sites of $Ti-(N(CH_3)_2)_3$ are emerged after the TDMAT exposure [31]. These reactive groups are mainly exist in the polymer subsurface and will react during the next reactant step leading to multilayer growth [30]. This film can then prevent the precursor from penetrating deep into the polymer bulk during the next $TDMAT/H_2O$ cycles, and ALD layer coalescence after some cycles leads to normal ALD growth [30]. These typical ALD growth mechanism can be indicated by surface morphologies evaluation of the PVA surface before and after TiO_2 ALD coating. The root mean square (RMS) surface roughness was calculated to be 659.83 pm for the uncoated PVA. The value decreased to 314.42 pm for TiO_2 nanosheet of 100 ALD cycles, and further reduced to 296.04 pm for TiO_2 layers prepared by 1000 cycles. The decrease of the surface roughness indicates that the ALD in the initial layer has been completed and the normal growth has started on the surface of the PVA [32,33], which is a basic requirement for the formation of free-standing nanosheets.

It is well known that the surface area is one of the most important factors affecting photocatalytic applications of nanomaterials [21,34]. In this regard, we estimated the surface areas of TiO_2 nanosheets (100, 300, 500, and 1000 cycles) with the help of AFM and the mass of TiO_2 nanosheets was normalized to 0.1 mg (by assuming the TiO_2 ALD density was ~3.9 g/cm³ [35–37]). The surface area of thin film (Fig. 3a) decreased by increasing the number of ALD cycles and corresponding thickness. To check the exact thicknesses of the nanosheets with different ALD cycles, we used AFM to probe the thickness at the edges of the nanosheets, as shown in Fig. 3b. A typical AFM image of the edge of TiO_2 nanosheet prepared with 100 ALD cycles is shown in Fig. 3c. In this work, the average thicknesses of the TiO_2 nanosheets produced by 100, 300, 500, and 1000 cycles were 11, 23, 34, and 80 nm, respectively. We also carried out XRD measurements to analyze the crystal structures of the nanosheets with different ALD cycles. The XRD results in Fig. SI-5 shows that the nanosheets do not have any detectable crystalline structure, which suggests that the TiO_2 nanosheets with various thicknesses from ~ 11 to ~ 80 nm are in amorphous phase. However, as it was mentioned before, increasing the stiffness of nanosheets can reflect more regular repetitive pattern of the atoms (i.e., locally ordered structure) in thicker nanosheets [25–29]. Unfortunately, XRD has detection limit of crystalline domains below 3–5 nm [28], and therefore no diffraction peak can be observed in XRD pattern.

Fig. SI-6 of supporting information shows the chemical composition of the TiO_2 nanosheet with 500 ALD cycles that represented by deconvolution analyses of XPS spectra of (a) O 1s and (b) Ti 2p. The peak of O 1s was fitted and divided into two subbands. The subbands at
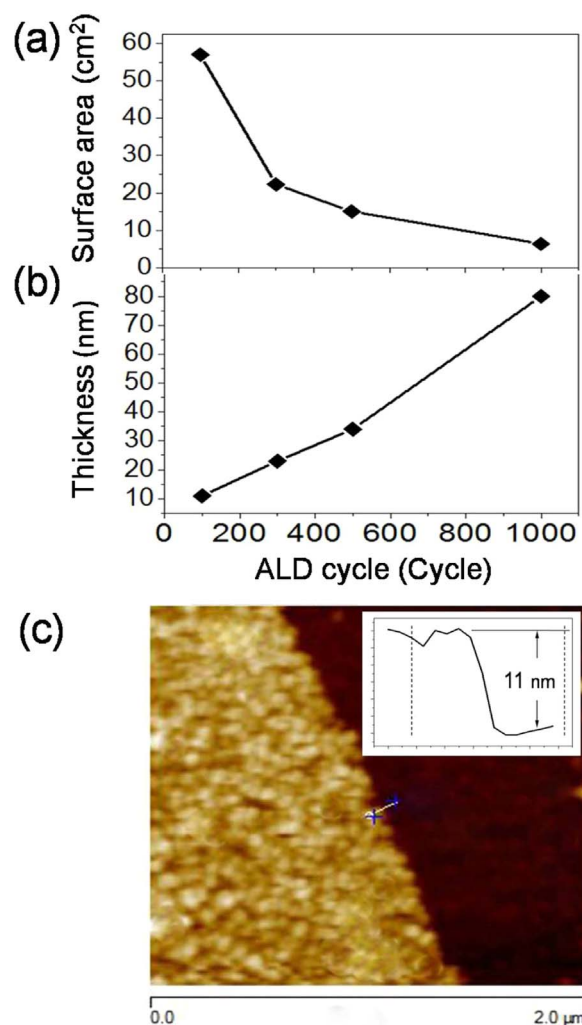

Fig. 3. The surface area (a) and the thickness (b) of TiO_2 nanosheets as functions of ALD cycle. The mass of the TiO_2 nanosheets was normalized to 0.1 mg. (c) AFM image of the edge of a TiO_2 nanosheet prepared by 100 ALD cycles.

the binding energies of 529.76 and 531.47 eV corresponds to oxygen atoms connecting to Ti^{4+} and Ti^{3+}, respectively [38–40]. Fig. SI-6b shows the XPS spectra of Ti 2p, with the peaks at the binding energies of 458.2 and 463.8 eV corresponding to $Ti^{4+}(2p_{3/2})$ and $Ti^{4+}(2p_{1/2})$, respectively. While both peaks shift to lower binding energies compared to the previous studies of 458.6 eV ($Ti^{4+}(2p_{3/2})$) and 464.3 eV ($Ti^{4+}(2p_{1/2})$) [38,40–42], suggesting the existence of Ti^{3+} in the sample [40,42]. Both spectra of O 1s and Ti 2p indicate the existence of oxygen vacancy-Ti^{3+} type surface state. The presence of Ti^{3+} at the surface of the TiO_2 are beneficial to photocatalysis, as it can react with the available dissolved O_2 and lead to formation of active oxygen species, such as superoxide radical anion $^•O_2^{\,-}$, hydroperoxyl radical $^•HO_2$, and hydroxyl radical $^•OH$, which are directly responsible for the degradation of the typical organic pollutants [43,44]. In addition, it has been reported that the photoelectrons can be trapped by existence of the surface defect (Ti^{3+}) leading to inhibition of e^- - h^+ recombination, which consequently has a contribution to increase the photocatalytic reactions [35,45].

MO degradation experiments were carried out to measure the photocatalytic activity of the TiO_2 nanosheets. Fig. 4a shows the enhancement of MO degradation by existence of TiO_2 nanosheets with different thicknesses. For all tests, the photocatalyst concentrations are kept constant at 0.017 mg/mL. The degradation follows a pseudo-first-order reaction with kinetics expressed by $\ln(C_0/C)=k \cdot t$, where t is the irradiation time, C_0 and C represent MO concentrations of the initial
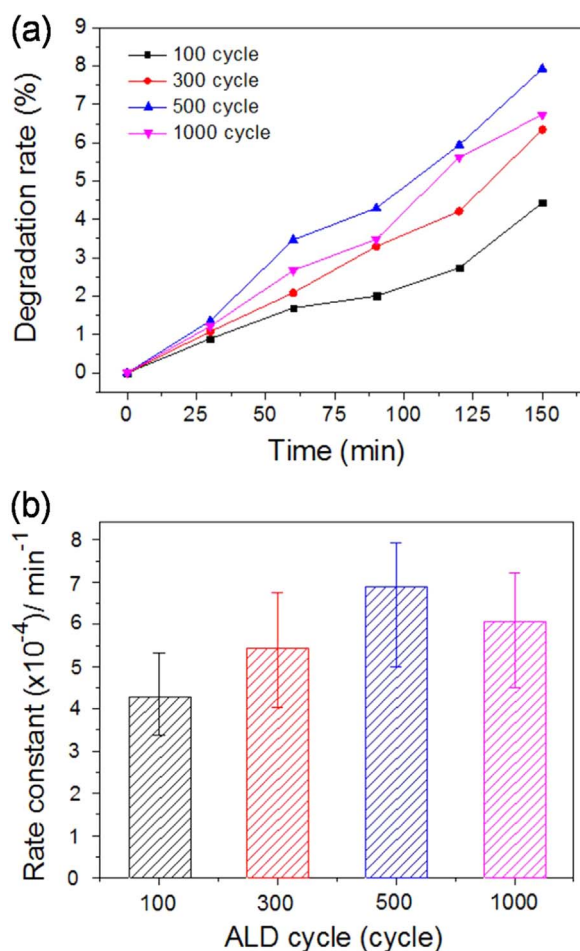
Fig. 4. (a) Photocatalytic performances of TiO$_2$ nanosheets, in term of MO degradation. (b) Corresponding degradation rates, calculated from (a).

4. Conclusions

Free-standing TiO$_2$ 2D nanosheets with various thicknesses from ~11 to ~80 nm have been succesfully fabricated by using ALD on PVA sacrificial layers. Morphological characterization confirms that the TiO$_2$ nanosheets synthesized with fewer ALD cycles are more flexible. With increasing thickness, the nanosheet becomes stiffer with increasing locally ordered structure in the nanosheets. These locally ordered structures in TiO$_2$ nanosheets lead to enhanced photocatalytic performance. The photocatalytic ability of TiO$_2$ nanosheets may also be promoted by the existence of Ti^{3+} defect. The results obtained in this work can have potential applications in various areas, including photocatalysis, water splitting, and dye-sensitized solar cells.

Appendix A. Supplementary material

Supplementary data associated with this article can be found in the online version at http://dx.doi.org/10.1016/j.pnsc.2016.08.010.

References

[1] H. Kim, Thin Solid Films 519 (2011) 6639–6644.
[2] R.L. Puurunen, Chem. Vap. Depos. 9 (2003) 249–257.
[3] W.-S. Jeon, S. Yang, C.-S. Lee, S.W. Kang, J. Electrochem. Soc. 149 (2002) C306–C310.
[4] K. Tapily, J.E. Jakes, D.S. Stone, P. Shrestha, D. Gu, H. Baumgart, et al., J. Electrochem. Soc. 155 (2008) H545–H551.
[5] V. Sammelselg, R. Rammula, J. Aarik, A. Kikas, K. Kooser, T. Käämbre, J. Electron Spectrosc. Relat. Phenom. 156 (2007) 150–154.
[6] R.W. Johnson, A. Hultqvist, S.F. Bent, Mater. Today 17 (2014) 236–246.
[7] K. Lee, D.H. Kim, G.N. Parsons, ACS Appl. Mater. Interfaces 6 (2014) 10981–10985.
[8] M. Osada, T. Sasaki, J. Mater. Chem. 19 (2009) 2503–2511.
[9] I.Y. Kim, Y.K. Jo, J.M. Lee, L. Wang, S.-J. Hwang, J. Phys. Chem. Lett. 5 (2014) 4149–4161.
[10] M. Naguib, O. Mashtalir, J. Carle, V. Presser, J. Lu, L. Hultman, et al., ACS nano 6 (2012) 1322–1331.
[11] R. Ma, T. Sasaki, Acc. Chem. Res. 48 (2015) 136–143.
[12] G. Huang, Y. Mei, Adv. Mater. 24 (2012) 2517–2546.
[13] X. Zhuang, Y. Mai, D. Wu, F. Zhang, X. Feng, Adv. Mater. 27 (2015) 403–427.
[14] M. Osada, T. Sasaki, Adv. Mater. XX (2012) 1–19.
[15] F. Wang, X. Wang, Nanoscale 6 (2014) 6398–6414.
[16] A. Fujishima, K. Honda, Nature 238 (1972) 37–38.
[17] F. Tian, Y. Zhang, J. Zhang, C. Pan, J. Phys. Chem. C. 116 (2012) 7515–7519.
[18] H. Xu, S. Ouyang, L. Liu, P. Reunchan, N. Umezawa, J. Ye, J. Mater. Chem. A 2 (2014) 12642–12661.
[19] M. Li, G. Huang, Y. Qiao, J. Wang, Z. Liu, X. Liu, et al., Nanotechnology 24 (2013) 305706 8pp.
[20] J. Tao, T. Luttrell, M. Batzill, Nat. Chem. 3 (2011) 296–300.
[21] K. Chen, Z. Jiang, J. Qin, Y. Jiang, R. Li, H. Tang, et al., Ceram. Int. 40 (2014) 16817–16823.
[22] N. Roy, Y. Sohn, D. Pradhan, ACS Nano 7 (2013) 2532–2540.
[23] Y. Xie, Z. Wu, Q. Wu, M. Liu, L. Piao, Catal. Today 225 (2014) 74–79.
[24] K. Lee, M.D. Losego, D.H. Kim, G.N. Parsons, Mater. Horiz. 1 (2014) 419–423.
[25] W. D. C. Jr, D. G. Rethwisch, Fundamentals of Materials Science and Engineering: An Integrated Approach, John Wiley & Sons Inc, United States. 2008.
[26] K.K. Chawla, Fibrous Materials, Cambridge University Press, Cambridge, United Kingdom, 1998.
[27] R.E. Shallman, R.J. Bishop, Modern Physical Metallurgy & Materials Engineering, Elsevier Science Ltd, London, England, 1999.
[28] K. Eufinger, D. Poelman, H. Poelman, R.D. Gryse, G.B. Marin, Thin Solid Films: Process Appl. (2008) 189–227.
[29] P.M. Ossi, Disordered Materials, Springer-Verlag Berlin, Germany, 2006.
[30] G.N. Parsons, S.E. Atanasov, E.C. Dandley, C.K. Devine, B. Gong, J.S. Jur, et al., Coord. Chem. Rev. 257 (2013) 3323–3331.
[31] Q. Xie, Y.-L. Jiang, C. Detavernier, D. Deduytsche, R.L.V. Meirhaeghe, G.P. Ru, et al., J. Appl. Phys. 102 (2007) 083521.
[32] R. Edy, X. Huang, Y. Guo, J. Zhang, J. Shi, Nanoscale Res. Lett. 8 (79) (2013) 1–79.
[33] S.M. George, Chem. Rev. 110 (2010) 111–131.

solution and after illumination, respectively [46]. Thus the pseudo first-order constant k can be calculated to evaluate the photocatalytic efficiency (Fig. 4b). In TiO$_2$ structure, the degree of crystallinity represented by the ratio between crystalline and amorphous phase is an important factor affecting photocatalytic activity [28]. Normally, it is believed that higher degrees of crystallinity are beneficial for the TiO$_2$ photocatalytic performance [28], but in present case the amorphous TiO$_2$ nanosheets still demonstrates photocatalytic activity possibly due to the surface defect, as discussed above. One may also notice that the photocatalytic performance increases with increasing thickness/ALD cycles for thinner nanosheets (Fig. 4b). This phenomenon can be explained as follows. Firstly, the thinner amorphous TiO$_2$ nanosheets have the higher state of disorder at atomic level, which suggests a major random structure, and the photocatalytic performance is relatively lower. With increasing ALD cycles, the nanosheets become stiffer, corresponding to higher level of local ordering, i.e. repetitive three dimensional patterns [28,29], and the photocatalytic activity is enhanced correspondingly. Secondly, the nanosheets made by 100 and 300 ALD cycles are flexible and can self-wrinkle, fold and roll. This leads to reduced contact area with solution and worsens the photocatalytic performance. In addition, it is worth noting that the TiO$_2$ nanosheet formed by 500 ALD cycles demonstrates the highest degradation rate of 0.00069 min^{-1}, as shown in Fig. 4a and b. The inconsistency is considered to be due to the difference in the contact areas: the 500-cycles sample should have a larger surface area compared to the 1000-cycles sample, if the weights are the same, as shown in Fig. 3a.

[34] H. Park, Y. Park, W. Kim, W. Choi, J. Photochem. Photobiol. C: Photochem. Rev. 15 (2013) 1–20.

[35] V. Pore, Atomic Layer Deposition and Photocatalytic Properties Of Titanium Dioxide Thin Films (Academic Dissertation), University of Helsinki, Finland, 2010.

[36] M. Rose, J. Niinistö, P. Michalowski, L. Gerlich, L. Wilde, I. Endler, et al., J. Phys. Chem. C. 113 (2009) 21825.

[37] A. Niskanen, K. Arstila, M. Leskelä, M. Ritala, Chem. Vap. Depos. 13 (2007) 152.

[38] M.L. Li, G.S. Huang, D.X. Wang, J. Zhang, J.J. Shi, Y.F. Mei, J. Mater. Chem. A 2 (2014) 6708–6713.

[39] W. Fang, M. Xing, J. Zhang, Appl. Catal. B: Environ. 160–161 (2014) 240–246.

[40] M. Xing, W. Fang, M. Nasir, Y. Ma, J. Zhang, M. Anpo, J. Catal. 297 (2013)

[41] S. Pan, Y. Zhao, G. Huang, J. Wang, S. Baunack, T. Gemming, et al., Nanotechnology 26 (2015) 364001 6pp.

[42] X. Zhang, H. Tian, X. Wang, G. Xue, Z. Tian, J. Zhang, et al., Mater. Lett. 100 (2013) 51–53.

[43] K. Vajda, Z. Kása, A. Dombi, Z. Németh, G. Kovács, V. Danciu, et al., Nanoscale 7 (2015) 5776–5786.

[44] A. Fujishima, X. Zhang, D.A. Tryk, Surf. Sci. Rep. 63 (2008) 515–582.

[45] K. Suriye, P. Praserthdam, B. Jongsomjit, Appl. Surf. Sci. 253 (2007) 3849–3855.

[46] A. Shafaei, M. Nikazar, M. Arami, Desalination 252 (2010) 8–16.

236–243.